REPORT DOCUMENTATION PAGE

AFRL-SR-AR-TR-03-

0263

1. AGENCY USE ONLY *(Leave blank)*	2. REPORT DATE	3. REPL... DATES COVERED
		01 APR 01 - 30 SEP 02

4. TITLE AND SUBTITLE
AN ADVANCED FREE FLIGHT RESEARCH FACILITY

5. FUNDING NUMBERS
F49620-01-1-0258

6. AUTHOR(S)
DR. P. M. SFORZA

7. PERFORMING ORGANIZATION NAME(S) AND ADDRESS(ES)
UNIVERSITY OF FLORIDA
GRADUATE ENGINEERING AND RESEARCH CENTER
SHALIMAR, FLORIDA

8. PERFORMING ORGANIZATION REPORT NUMBER

9. SPONSORING/MONITORING AGENCY NAME(S) AND ADDRESS(ES)
AFOSR/NM
4015 Wilson Blvd, Room 713
Arlington, VA 22203-1954

10. SPONSORING/MONITORING AGENCY REPORT NUMBER
F49620-01-1-0258

11. SUPPLEMENTARY NOTES

12a. DISTRIBUTION AVAILABILITY STATEMENT
APPROVED FOR PUBLIC RELEASE, DISTRIBUTION UNLIMITED

12b. DISTRIBUTION CODE

13. ABSTRACT *(Maximum 200 words)*

This report documents activities to install a tomographic density station into the Aeroballistic Research Facility (ARF). The objective of this research grant was to provide new insights into fluid dynamic research and design since this technology has the ability to characterize the spatial and temporal density profiles around the projectile/model. In this section, an overview of the current measurement capabilities ARF are discussed as stand alone techniques and we reintroduce the advantages of combining them are described.

20030731 085

14. SUBJECT TERMS	15. NUMBER OF PAGES
	30
	16. PRICE CODE

17. SECURITY CLASSIFICATION OF REPORT	18. SECURITY CLASSIFICATION OF THIS PAGE	19. SECURITY CLASSIFICATION OF ABSTRACT	20. LIMITATION OF ABSTRACT

Final Report

An Advanced Free Flight Research Facility

Contract Number: F49620-01-1-0258

Submitted to:

Major William Hilbun
Air Force Office of Scientific Research
NI/DURIP
801 North Randolph Street, Room 732
Arlington, Virginia 22203-1977

From:

University of Florida
Graduate Engineering and Research Center
Shalimar, Florida

Principal Investigators:

Dr. P. M. Sforza
Dr. Chris Anderson

June 20, 2003

1. Introduction

This report documents activities to install a tomographic density station into the Aeroballistic Research Facility(ARF). The objective of this research grant was to provide new insights into fluid dynamic research and design since this technology has the ability to characterize the spatial and temporal density profiles around the projectile/model. In this section, an overview of the current measurement capabilities ARF are discussed as stand alone techniques and we reintroduce the advantages of combining them are described.

1.1 Current ARF Measurements

The purpose of the ARF is to advance basic aerodynamic knowledge and define aerodynamic performance, stability, and control parameters for hypervelocity missiles, advanced ammunition, high fineness ratio penetrators, submunitions, and many other types of flight vehicles. The ARF is an enclosed indoor firing range used to examine the exterior aerodynamics and ballistics of various projectiles in free-flight. Construction on the facility began in 1973, and it became fully operational in 1976. It has been in continuous use ever since. The facility contains model measurement equipment, a launch room, a blast chamber, an instrumentation control room, and the instrumented range. The instrumented range of the ARF is 207 meters long. It has a 13.4 square meter cross section for the first 69 meters and a 23.8 square meter cross section for the remaining length. There are 131 locations available for instrumentation sites, each having a 1.52 meter physical separation. Presently 50 sites are used to house orthogonal shadowgraph stations. An example photograph of a projectile going down range is shown in *Figure 1.*

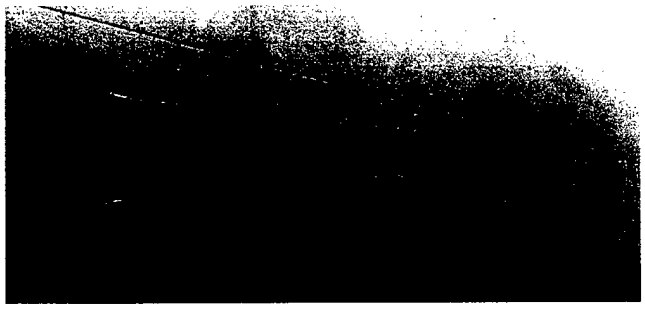

Figure 1. *Example Photograph From ARF. Catenary Wires Not Shown.*

These stations are used to determine the projectiles' free-flight orientation, spatial position and time location in flight. Each station has two cameras, one located along the wall and one in the floor. A spark source is generated for each camera as the projectile passes through an infrared beam. This high intensity light bounces off photo-reflective screens, creating a shadowgraph image on the film. The shadowgraph is created by changes in flow field density about the projectile..

Each photo-reflective screen also has four beads at precisely measured locations along catenary wires. Using these wire and bead locations, the orientation and location of the projectile can be measured. A small reference pin is inserted into the projectile's base and is used to determine the roll rate of the projectile. A time stamp for each camera is also recorded. This data is used to create a six degree-of-freedom trajectory, which is then processed by parameter identification computer algorithms to analyze the aerodynamics, stability, and performance of the projectile. By testing models with slightly modified configurations, the researcher can then begin to understand the impact the design has on performance. The shadowgraph images are also used to measure flow field features like shock wave shapes, etc.

The measurement accuracy of the ARF is very good. Projectile position in the vertical and cross range planes can be measured to within +/-1 mm. Horizontal position along the flight path can be measured to within +/-1.5 mm. Angle of attack and yaw angles are accurate to within +/-0.1 deg. Roll orientation, depending on the projectile's spin rate, can be measured to within +/-3 deg.

1.2 Time Evolving Density Measurements

Independent of the ARF application, newly developing technology at the UFGERC now permits researchers to measure the density of a fluid flow both spatially, and in time, using non-intrusive, optical techniques. While many researchers have worked on obtaining quantitative information on the density fields around projectiles, including in the ARF, limited success has been obtained in developing a reliable instrument that could be used in such difficult test environments. To the best of our knowledge, no techniques, other than that developed at the UFGERC and discussed for the first time in this proposal, have demonstrated the ability to measure time-resolved density on the time-scales consistent with high speed events. Currently, the University of Florida is pursuing a patent for this technique prior to making its availability widely known.

Two recent events at the UFGERC have shown that a new optical approach can be readily applied to high-speed, density analysis. First, Dr. Land and Dr. Anderson demonstrated that an emerging technique in the aero-optics community can be reliably, and accurately applied to density characterization for many fluid applications[1-2]. While the sensor approach that was applied is not unique, the engineering details of constructing a 3-D density measuring station were new. Second, Dr. Anderson developed a technique by which multiple frames (currently 4) of density data can be gathered at rates up to 500,000 frames per second [3]. This step enables the researcher to gather density information for unsteady fluid flow applications with a minimal increase in the expenditure for the test instrument.

To date, the UFGERC has applied the new technique to three different two-dimensional fluid flow problems: 1) compressible flow over a cavity, 2) flow in a shock tube, and 3) choked flow from an axisymmetric nozzle. Density profiles for each have been extracted with estimates on accuracy being better than +/- 3%. For any given application, the density profile is measured using a grid of 100 x 100 spatial points. As an example, the cavity flow measurements have a spatial resolution on the order of 0.5 mm. Temporally resolved densities have been applied to the cavity flow application with time between images ranging between 2 μsec and 250 μsec; since the flow in the cavity oscillated relatively slowly with a 2 kHz cycle time, we operated the instrument with 50-100 μsec frame separations. *Figure 2* illustrates recent results that have been obtained for a highly unstable cavity flow. The density technique is beginning to provide insights into the cavity flow dynamics that have never been observed before.

The density measurement capability at the UFGERC is currently limited to two-dimensional (either planar or axially symmetric flows). But the solid ground work that has been performed demonstrating the utility of the instrument gives us the confidence to take next logical step which is to apply the approach to three dimensions by incorporating well established tomographic techniques. The fact that this instrumentation system can be coupled to current ARF measurement capability is clearly a bonus. As is discussed later, the instrumentation proposed for the Advanced Free Flight Research Facility will permit accurate imaging of the flow around a 3-D projectile with temporal resolution on the order of 1 μsec.

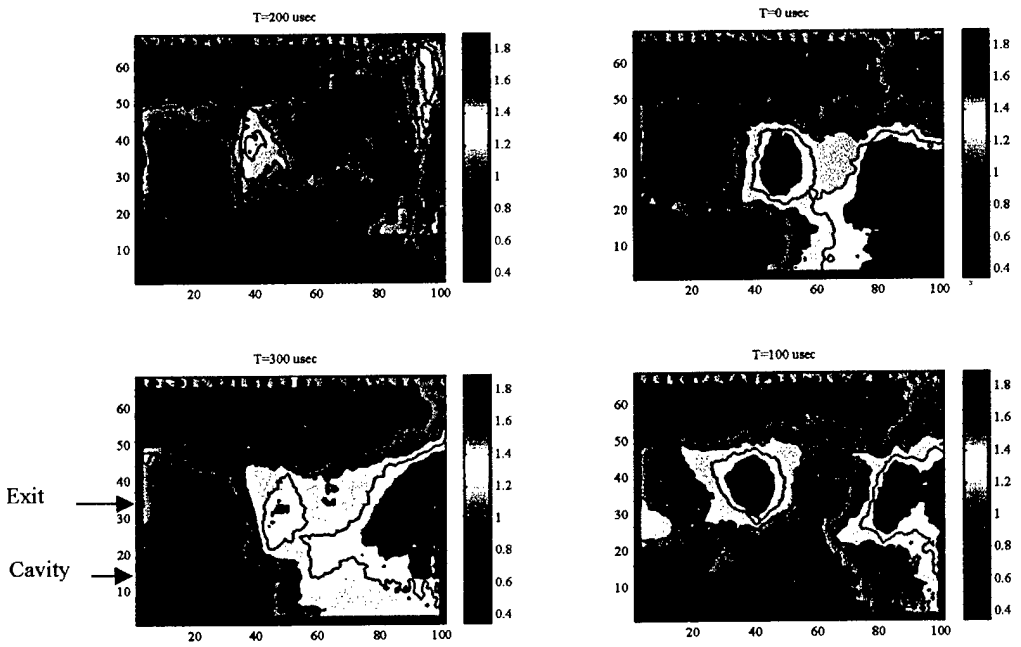

Figure 2. Four Time Resolved, Relative Density Images From Cavity Flow. Density relative to ambient room density. Exit Mach is 1.0 and length to depth ratio is 4.0. Cavity is illustrated by dark lines on border. Note evidence of cavity filling and dumping.

1.3 Advantages Of Combining Measurements

Given the advances in computational fluid dynamics (CFD), most of the research/design verification work performed in the ARF has been simulated with one of the array of currently available codes. For the aerodynamic designer or researcher, however, validation of the designs created by these models is always crucial prior to proceeding further. In cases where the forces and moments measured in the ARF agree with the CFD model, no additional tools are needed. However, in advanced aerodynamic design or research, the capabilities of the CFD code are often pushed to a point where one is never certain if imbedded code assumptions are valid. This is especially true for unsteady aerodynamic problems, where the CFD codes are not as mature.

A frequent occurrence is the observation of discrepancies between the CFD results for the model and the test results for the model in the ARF. While CFD is providing detailed predictions of pressure, temperature, density, and velocity at all points in the flow, researchers currently can only see the effects that the integrated surface pressures have on the test projectile. Now, suppose that time-resolved density measurements can be performed at all points around the free flight object. While a complete range of aerodynamic properties cannot be obtained, we can

definitely gain significant insight into the physics of the problem. In some applications, for example, we may be able to independently estimate the surface temperature profile, which when combined with the density, would enable local surface pressure distributions to be derived from measurements. By integrating the pressure profile, the total forces/moments can be compared using the existing ARF measurements. We recognize that in many applications it will be difficult to measure temperature at the surface but simply want to illustrate that the density field measurements would provide one more important piece of a complex unknown problem.

From a fluid dynamics perspective, the measurement of time-resolved, 3-D density profiles presents interesting possibilities. At first look, one rapidly concludes that this would provide a quantitative tool to verify at least the density profile obtained via computational fluid dynamics. We believe, however, that the benefits potentially far outweigh simply verifying CFD calculations. Suppose, for example, that the density profiles are measured at two closely spaced time points, relative to the rate of change of density. By using the spatial and time profiles of density, we can recover $\delta\rho/\delta x$, $\delta\rho/\delta y$, $\delta\rho/\delta z$. $\delta\rho/\delta t$, which show up as primary components in the continuity equation. Other application specific, aerodynamic information may be available that can be combined with the above to allow further unwrapping of the complex issue of fluid diagnostics.

As aerodynamic analysis tools are moving further into the unsteady state arena and as the use of CFD codes proliferates, we believe that it is important to establish a research facility that can truly measure key aerodynamic parameters. As advances are made in other measurement techniques, these can be added to provide further insight into previously intractable aerodynamic problems.

2. Non-Invasive, Time-Resolved Density Measurements

Density based flow visualization has played an important historical role in helping refine fluid dynamic theory and design practices [4]. Referring to ***Figure 3a***, a planar optical wave interrogates a flow field of interest. Localized variations in the fluid density give rise to minute, optical index of refraction, $n(x,y,z)$, changes which in turn, modulates the local phase of the optical beam as it traverses through the field. The phase change of a non-homogeneous flow field is related to refractive index by [4]

$$\frac{\phi(x,y)}{2\cdot\pi} = \frac{1}{\lambda}\cdot\int_{\zeta_1}^{\zeta_2}[n(x,y,z)-n_o]\cdot dz\ . \qquad (1)$$

Compressible flows, i.e., those at speeds above about Mach 0.5, consist of regions of varying fluid densities. For a gas, this fluid density is related to the optical indices of refraction by[4]

$$n(x,y,z)-1=K\rho(x,y,x), \qquad (2)$$

where $\rho(x,y,z)$ is the density of the fluid and K is the Gladstone-Dale constant (a property of the gas). We also note here that known gas compositions are required to determine K. It some applications, such as hypersonics, it may be required to iteratively estimate the compositions from CFD and then apply that to density field measurements.

For high-speed, compressible flows, much of the work in optical diagnostics of flow fields has centered around qualitative measurements, such as those produced by Schlieren, shadow-graph, or dark central ground techniques. Recent advancements in high speed digital cameras has enabled the capture of time-resolved imagery [5-6]. This type of imagery is not quantitative since it cannot be used to reconstruct $\rho(x,y,z)$, but important flow features, and their time evolution, can be ascertained. Examples of such features include shock locations, vortices, and regions of turbulence or any region containing a strong density gradient as is evident from the image shown in ***Figure 3b***. Our proposed instrumentation system aims to provide both quantitative and time-resolved density information.

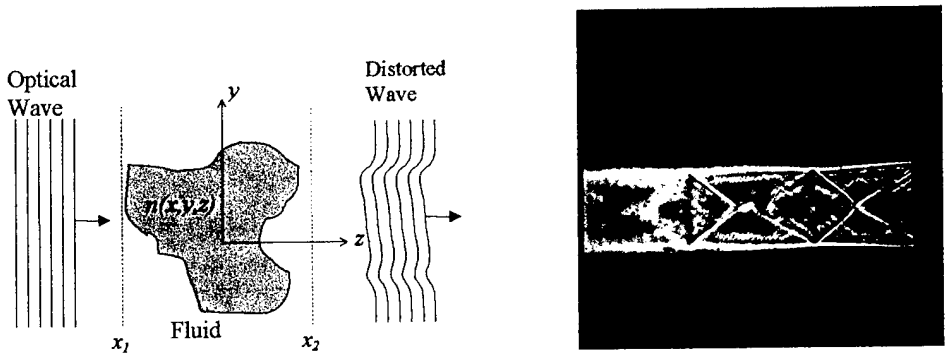

Figure 3 – a) Optical Interrogation Of Flow-Field, b) Typical Imagery

2.1 Quantitative Density Reconstruction

Equation (1) shows that the measurable quantity, optical phase, is the integral of the density profile. To obtain the three dimensional density profile, $\rho(x,y,z)$, we must use tomographic reconstruction techniques [7-8]. ***Figure 4*** illustrates a tomographic density station where four optical beams interrogate the flow field from different directions; in general eight to ten optical beams coming from different directions are required for sufficient accuracy [2]. If accurate phase measurements are obtained simultaneously from the N directions then we are left with a set of measurements $\theta_i(x,y)$ where *i* denotes the viewing direction. Using well established tomographic reconstruction techniques, it is straightforward to recover $\rho(x,y,z)$. If the optical phase profile can be measured repeatedly, with temporal resolution consistent with the highest temporal changes in density, then a complete sampling of $\rho(x,y,z,t)$ can be obtained.

While the advantages of measuring time-resolved density fields have been well known, the engineering aspects have previously been beyond realistic reach of researchers. Specific issues causing difficulty are described below:

Measurement Of Phase – Most optical flow visualization techniques (Schlieren, Shadowgraph, Dark Central Ground, etc.) do not accurately measure $\theta_i(x,y)$ but rather provide images showing where rapid rates of change of the phase occur. To perform tomographic reconstruction of density, however, we must have accurate phase recovery. Historically, this has been attempted with optical interferometers of holographic systems but the difficult alignment requirements of the techniques, and the great expense of the optics, have made it extremely difficult to establish tomographic density stations. As will be discussed in the next subsection, a new technique using Shack-Hartmann sensors [9] allows very robust and accurate measurement of optical phase and the cost per view direction is low.

Time Resolution – Over the last 10 years, high speed cameras (both film and CCD) have been developed that allow images to be recorded with time spacings of less than 10 μsec. These cameras have been applied at the UFGERC and elsewhere to observe time-evolving flows but with non-quantitative techniques. A major difficulty in using these cameras for a tomographic density station is their cost. One of the more advanced CCD cameras at this time captures 8 time-resolved images but at a cost of

$250,000 per camera. When assembling a tomographic density station with 10 cameras, the total cost is unrealistic. Using a new development described below, we can record images with time spacing of 2 μsec or greater but at a cost less than $15,000 per camera. To totally outfit the density station with cameras and thus costs less than the cost of a single camera previously.

Post Processing – Quantitative optical phase measurements, when they have been performed, have been difficult to extract from the raw data. Many attempts are underway to extract this information from holograms or interferograms but the effort is not straightforward. Using the Shack-Hartmann sensors, this phase recovery process is very easy and algorithms are now well established.

It is worth mentioning that under two special conditions $\rho(x,y,z,t)$ can be recovered using a single optical view rather than the tomographic station shown in *Figure 4*. The first condition is when the flow field is two-dimensional and thus $\delta\rho/\delta z = 0$. In this case, the index of refraction is constant with respect to z and Eqn (1) is solved directly once the phase is measured. The second case occurs when the flow has axial symmetry. In this circumstance, a single optical phase measurement can be made and the density profile reconstructed using either Abel's inversion principle [4] or the view is simply repeated (measurements from all angles are the same) and sent to a tomographic reconstruction algorithm.

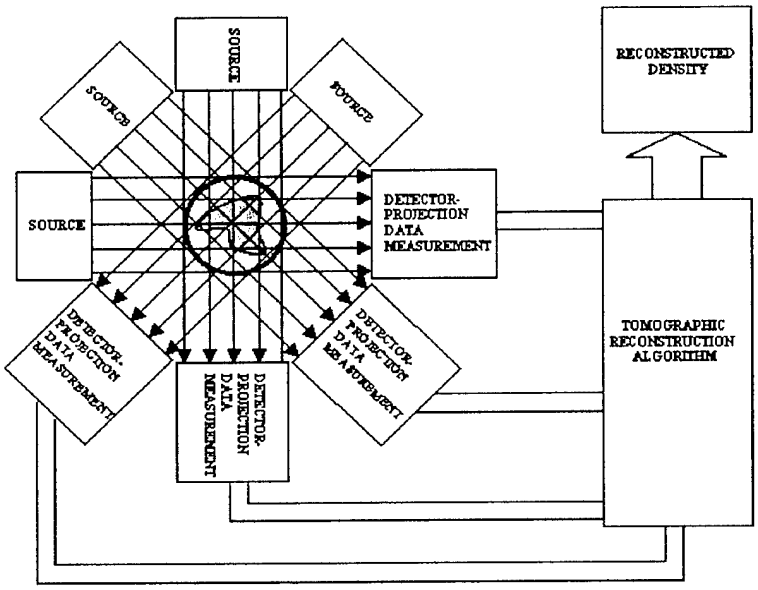

Figure 4 - Tomographic Systems

2.2 Time-Resolved Shack-Hartmann Sensors

Shack-Hartmann sensors, which are one class of wavefront sensors, sample the gradient of the distorted optical phase front. This type of sensor has found a niche in adaptive optical systems for atmospheric aberration compensation in astronomical telescopes. In these applications, the wavefront sensor measurements are used in a closed loop control system along with deformable mirrors to compensate for atmospheric induced distortions. While relatively new for general purpose optical wavefront measurement, the reduction in fabrication cost of producing the required lenslet arrays have allowed two companies to offer off-the-shelf-instrumentation for wavefront analysis [10]. In addition to UFGERC, other researches are starting to apply these sensors to flow field diagnostics. The UFGERC wants to significantly advance the capabilities of these systems, however, by developing a true 3-D density measurement system operating at microsecond frames rates. To date, 2-D tomographic techniques have been demonstrated at millisecond rates [11] and a 2-D, non-tomographic system at microsecond rates [3]. We believe that the groundwork has been set for practical transition to the time-resolved, density station.

In the Hartmann sensor, the distorted wave is broken into a spatial array of samples, or sub-apertures, by an array of lenslets as shown in *Figure 5a*. Each sub-aperture is brought to focus on a detector array positioned in the back focal plane of the lenslets. Since the lateral position of the spots depends upon the local tilt of the incoming wave, the array of measurement

spot displacements represents the wavefront gradient sampled at the locations of the lens array sub-apertures. *Figure 5b* illustrates the raw camera output for the spots. To implement the tomography system shown in *Figure 4*, we require one laser diode transmitter and one lenslet receiver for each view.

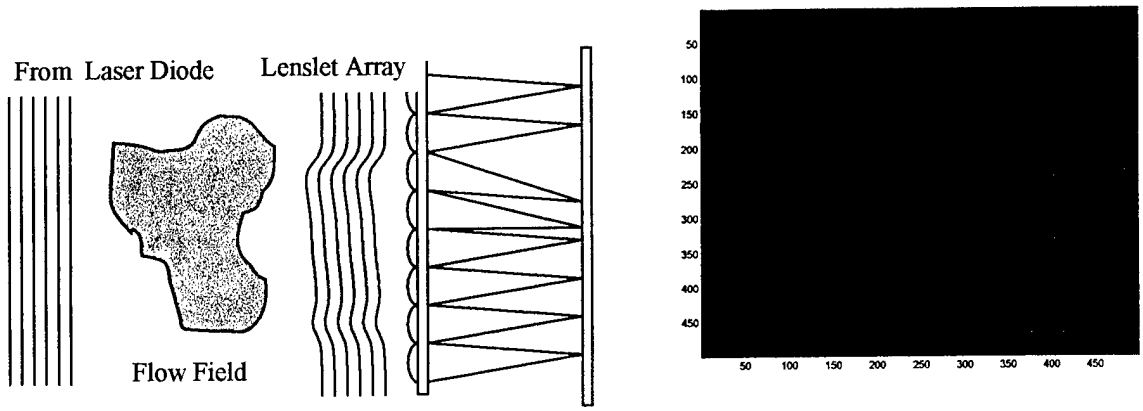

Figure 5 - a) Shack-Hartmann Lenslet concept, b) Camera Spots

Until recently, a time-resolved Hartmann sensor was made by reading the spot images out of the camera at high-speed. Unfortunately, camera frame times are typically greater than 1msec, thus the temporal resolution is coarse. The UFGERC has developed a technique to rapidly multiplex four, time-resolved images onto a slowly operating CCD camera. The key to understanding the approach is to recognize that a single wavefront sensor uses only a small portion of the sensor array at any given time. *Figure 6a* shows an expanded, 3-D view around the region of one of the spots. Each of the square boxes shown represents one CCD detector element. For this type of sensor, it is the location of the spot on the detector array that permits the needed information to be determined. From this figure, we see that a good deal of detector space is wasted in order to allow the sensor to measure severe wavefront distortions.

As *Figure 6b* shows, it is possible to multiplex many more spots into a given region if the sensor design requirements are understood at the beginning. Our current system allows four spots to be multiplexed into a 9 x 9 detector region. For the first image, a single Shack-Hartmann image is produced with one spot in the 9 x 9 area. For the second image, the spot is displaced by a known amount (4 pixels in our current design) and the second image is recorded. This is repeated N times: N=4 in our current design but this can be increased with design tradeoffs.

Software has been written to accurately locate the center of each spot, thus effectively allowing N Shack-Hartmann images to be collected on a single camera.

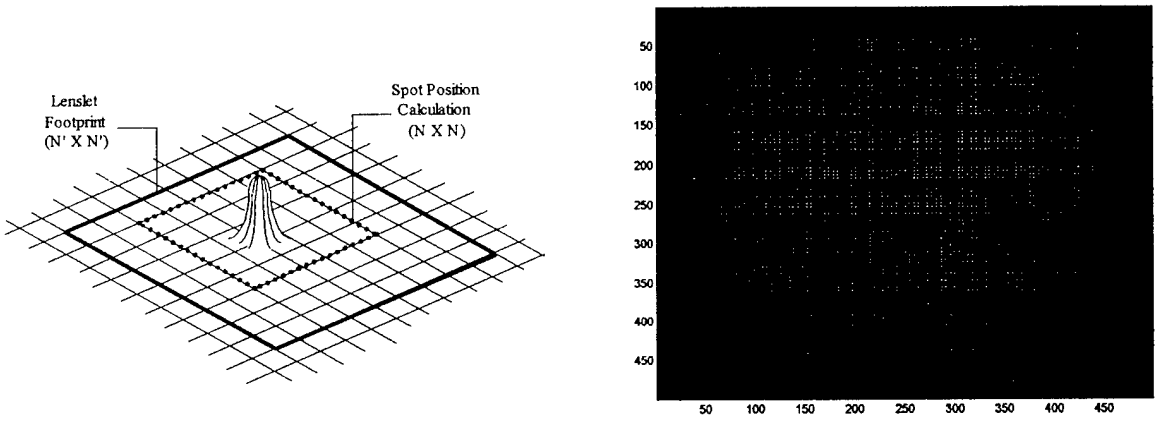

Figure 6 – a) Zoom around one lenslet spot, b) spot image showing each lenslet having four multiplexed images.

In order to make a time-resolved sensor using this technique, we must rapidly multiplex the N images while moving the central spot location a known amount between frames. In concept, this can be accomplished by 1) moving the lenslet array between exposures, 2) mechanically moving the optical beam between exposures, or 3) changing the source location between exposures. The third is our preferred approach since it can be effected with no mechanical motion. Using a low cost laser board with four laser diodes, we move the spots by turning on a different laser for each new exposures. For the first image exposure, Laser 1 is turned on for a brief (0.5 microsecond) period and then turned off. This produces one exposure on the camera. Next, Laser 2 is turned on some known time later (2 microseconds in our case) to produce the second exposure. This is repeated N times. Since the lasers can be turned on and off at very high rates, this can be used to produce N images, very rapidly, using a normal CCD camera with slow frame rates. The cost of the laser diodes and electronics is typically less than $500 thus making high-speed sensors practical.

3. Original Research Plan

The funds provided from the DURIP grant allowed the researchers to purchase the equipment needed to establish the described advanced density station in the ARF and to also provide real-time feedback on a projectile's position and attitude prior to, and leaving, the density station. *Figures7* illustrates the density measuring station concept and *Figure8* is a 3-D rendering of the layout in the ARF. Inside of the density station, ten cameras are used to record the multiple, Shack-Hartmann views needed for tomography. In addition, there is the associated optics, electronics, etc. that accompanies the cameras. Before and after the station, two electronic, orthogonal shadowgraph stations must be constructed to simultaneously calculate model position during the test. The basic instrumentation needed to perform these tasks include digital cameras, frame grabbers for digitizing the camera information, PCs to operate the frame grabbers and network the data, lenslet arrays to implement the Shack-Hartmann approach, and then supporting optical and mechancial equipment.

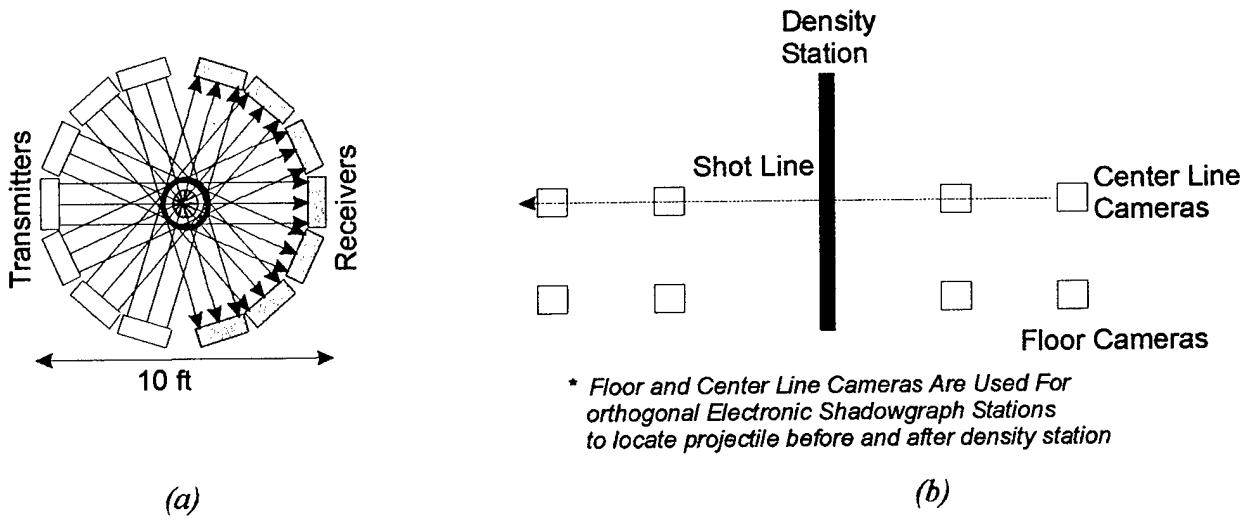

Figure 7. *a) End view of tomographic density station (all views not shown) and b) side view of tomographic density station along with supporting orthogonal shadowgraph stations.*

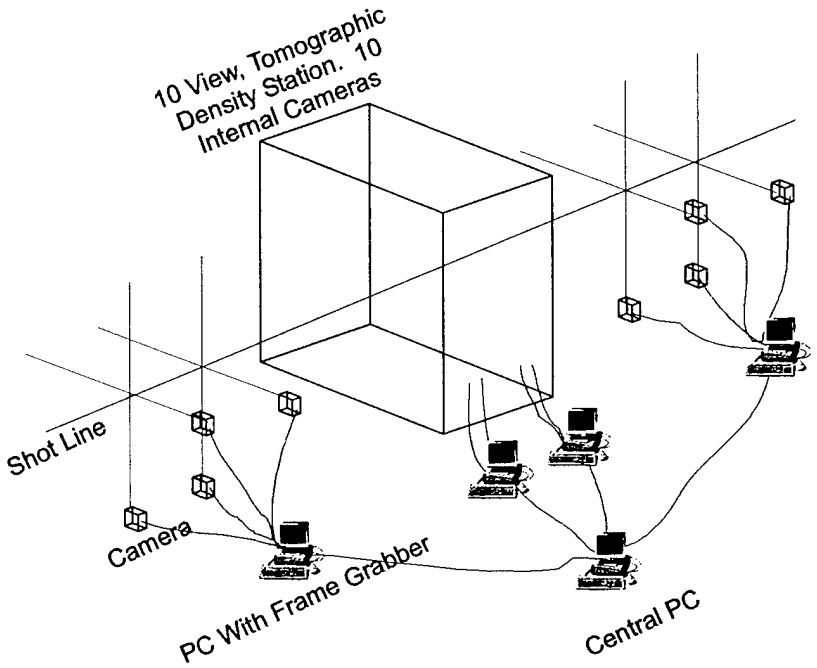

Figure 8. *Layout of ARF Density Station With Supporting Orthogonal Position Determination Before, And After The Test Station. Also illustrates subset of required PC stations for image capture.*

Our objectives where to perform final design for all the equipment, procure, assemble, and then test. As we address later, issues arose that caused setbacks in this original plan.

4. Procured Equipment

In this section, we discuss the equipment that was procured under this grant and the governing reasons for selecting the equipment.

4.1 Camera

The Redlake Model ES 1.0/SC was selected for this application with 1024 x 1024 CCD elements. One of the primary motivations for selecting this particular camera was its ability to perform in line transfer mode which allows to collect two images spaced only microseconds apart. For our application, we produce four spots on a single camera image, transfer that image to on-board storage, and then capture a second set of four images. Using our time multiplexing technique, this enables the recording of eight time-resolve frames of data in the Shack-Hartmann sensor. All of the cameras collected together for initial testing is shown in Figure 9.

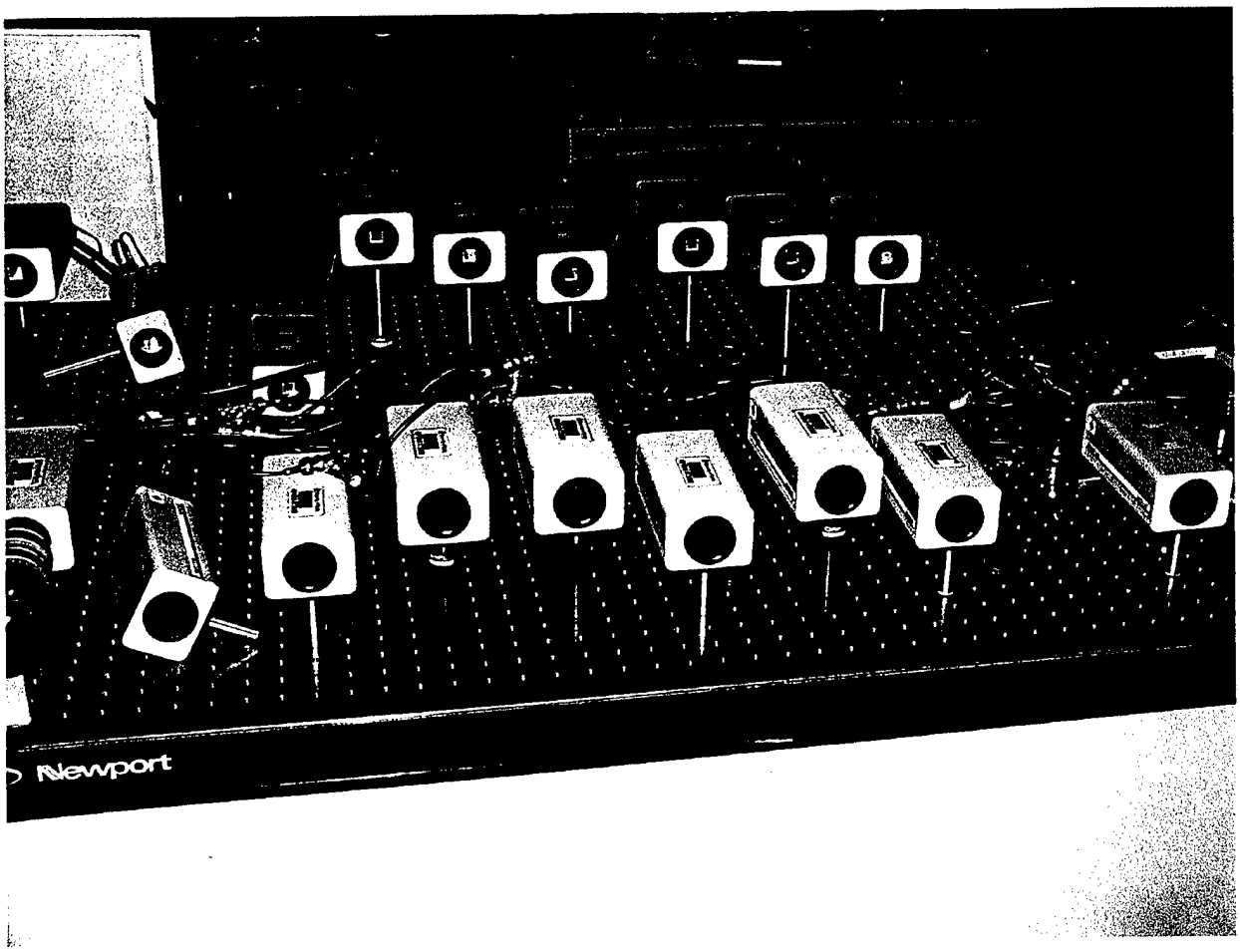

Figure 9. Cameras Assembled For Initial Testing

4.2 Data Capture & Frame Grabber Electronics

Synchronizing all cameras to capture data at the same instant and transfer that information to a central processing unit turned out to be a daunting task. In the tomographic system, 10 cameras are to be used thus 10 frame grabbers are also employed. To simply acquisition of the data, we purchased a completely integrated (but custom) system from Zedec Technologies (www.zedec.com) in North Carolina. A photograph of the camera controllers in shown in Figure 10.

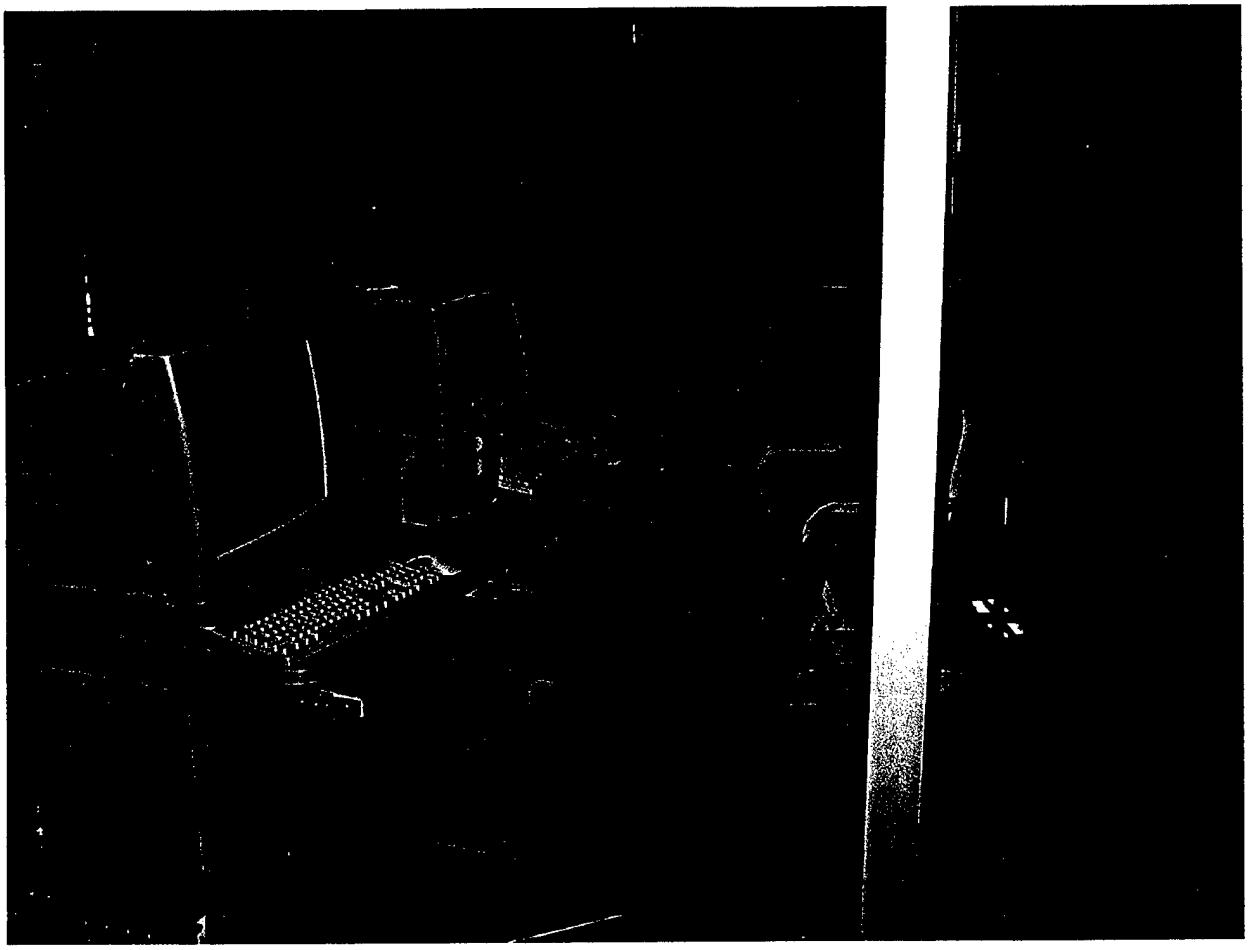

Figure 10. Photograph of Camera Controllers

4.3 Laser Diode and Driver Board

Two lasers were used for this project: A Sanyo 5 mW, 670 nm red laser diode(DL3149-056) and a Sanyo 75 mW, 780 nm infrared laser diode (DL-7140-201). While the red laser diode was a version that we had used previously, we ran into difficulties with its use as discussed later. Ultimately, we elected to only use the IR laser diode.

A custom drive electronics board was developed to mount and time the four laser diodes. A silk screen layout is shown in Figure 11. Control signals are input into the clock data which then control counters. For each TTL level high input, the counter is moved forward (which then selects the next laser diode to turn on) and the diode is supplied power for the duration of the clock pulse. For our application, the clock pulse is 250 nsec in duration. Whenever it is desired to turn on the next diode, a new clock pulse is issued. We used a Textronix arbitrary waveform

generator to provide programmable clock pulses of arbitrary separation. In addition, a clear board control is providing which insures that the laser diode sequence always begins at the first laser.

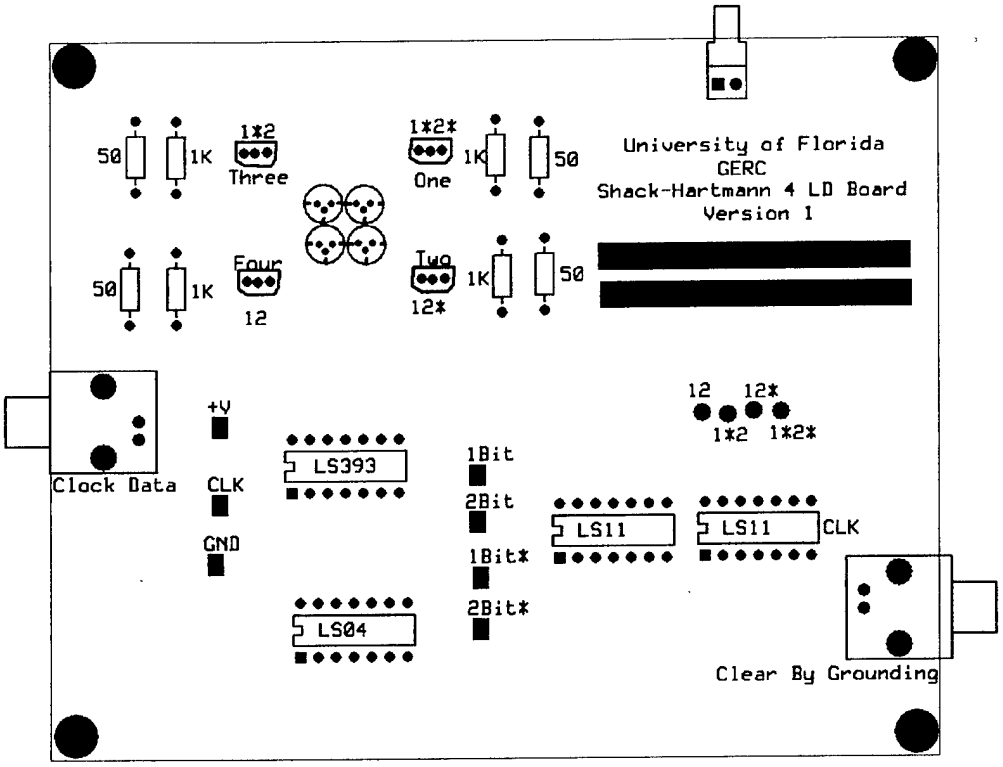

Figure 11. Silkscreen Layout Of Laser Diode Driver Board.

4.4 Telescopic Optics

As illustrated in Appendix A, there is a telescopic optics section between the flow field and the camera with embedded lenslet. This is a simply 4F telescope design and is implemented with achromatic lenses to minimize spherical aberration.

4.5 Lenslet Array & Mount

Selection of the lenslet array is one of the critical issues in designing the Shack-Hartman lenslet. The purpose of the spreadsheet in Appendix A is carefully balance focal length and lens f# to simultaneously achieve a good design. We choose the 0100-1.7-S-A lenslet from Adaptive

Optics Associates for a number of reasons. First, this focal length provided adequate sensitivity but also was ideal so that the lenslet could be mounted directly on top of the CCD chip in the camera; i.e., the optical path length from the chip window to the sensor was 1.7 mm. This lenslet is 100 microns in diameter thus producing a high f/# of 17. Since the detector spacing is 8.6 microns, this implied that the lenslets would be spaced by 11.6 pixels on the CCD. This also means that individual spots would be separated by 11.6 pixels nominally. For mounting, we replaced the lens bulk head in the original camera with an aluminum tube. Our lenslet was then inserted inside a 2nd aluminum tube which was then inserted into the bulk head tube. This allowed us to slide the lenslet into the camera until it just touched the sensor cover. Once inserted, the tube was rotated to align the lenslet array with the CCD array in rotation angle.

5. Initial ARF Testing

Our original plans called for purchasing the equipment, completing a single view of the tomographic system, and then testing in the ARF with a small caliber projectile. Once that was completed, we were to install an orthogonal test station and then finally the tomographic system. As we discuss here, these changes were modified significantly for a number of reasons.

Figure 12 shows the simple layout of original test and Figure 13 shows an aerial view of the ARF facility to provide perspective. A 0.22 caliber rifle was mounted up range about 100 feet from the optical test station. Optical sights were then used to align the rifle with the center of the test region which was a 2 " by 2" square. Infrared screens where then intalled up range from the optical system to provide triggering information. Eight time resolved images where collected at 10 microsecond spacings.

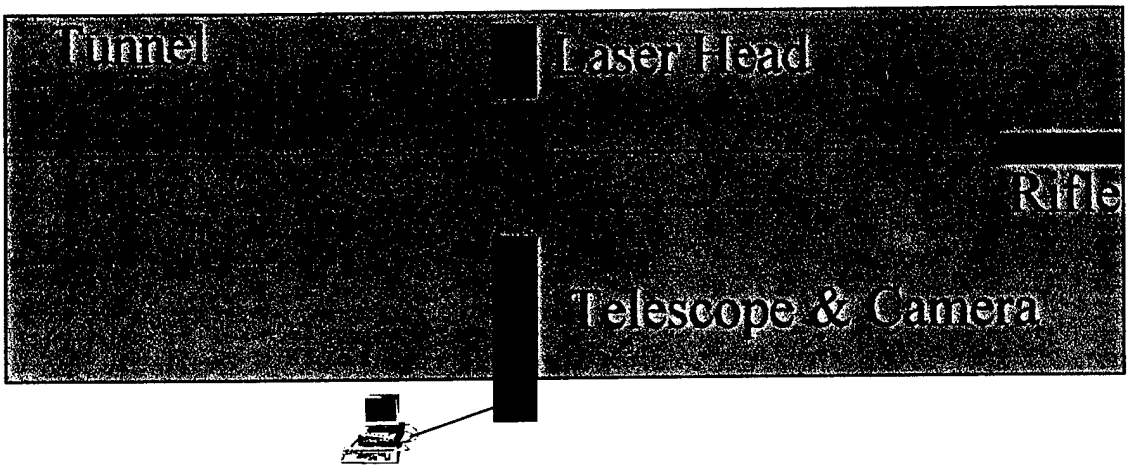

Figure 12. Layout of ARF Single View Test

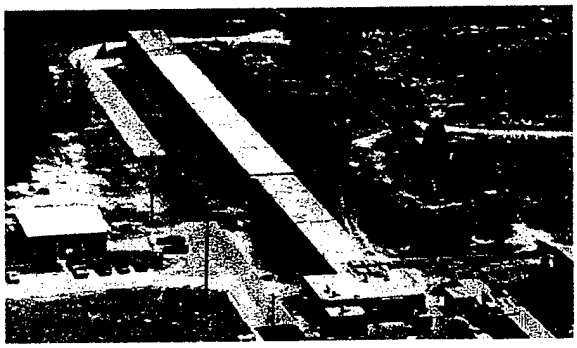

Figure 13. Aerial View of ARF.

Unlike other tests performed with the Shack –Hartmann sensor at the University, this projectile was supersonic and thus contained shock waves which we know apriori. To reconstruct the phase information from the spot displacements in the sensor, care has to be maintained across discontinuities in phase, which occurs at shock boundaries. The planned approach was to calculate the phase wavefront inside the shock cone, and outside the shock cone separately to avoid this discontinuity. To be able to locate the shock wave, we developed software to process the image solely for the purpose of shock location. Figure 14 shows the locations of discontinuities for 8 frames of the projectile data. We can clearly see the projectile enter and leave the optical window.

ARF Projectile/Shock Tracking

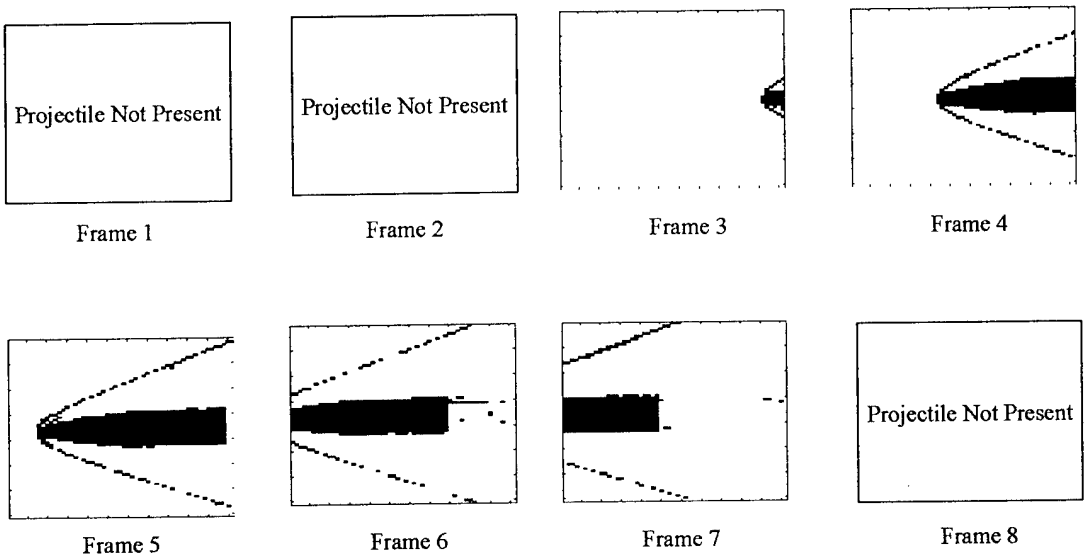

Figure 14. Shock Tracking

With knowledge of the shock locations, we can then extract the phase information between the regions of discontinuities. Figure 15 shows a gray scale representation of the optical phase information with the dark center region being where the opaque projectile is located. We only show four images here size reasons. A different representation is shown in Figure 16 for only the topside of the phase front in a color contour form and Figure 17 shows a zoom of the wavefront in one region. These phase results appeared to be close to what was expected.

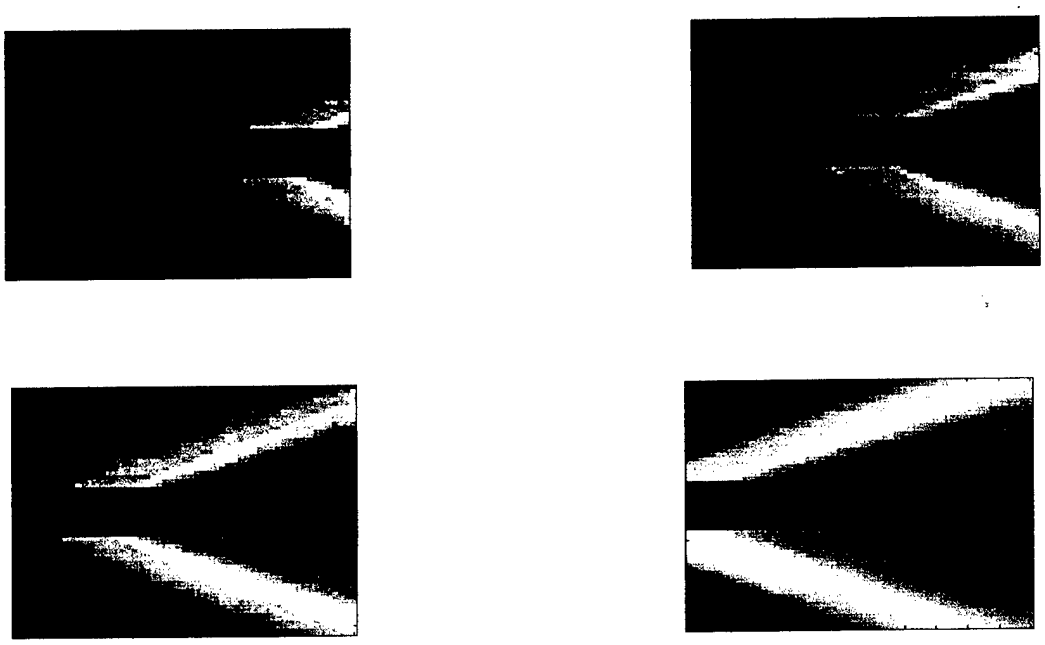

Figure 15. Gray Scale Images From Reconstructed Phase Information.

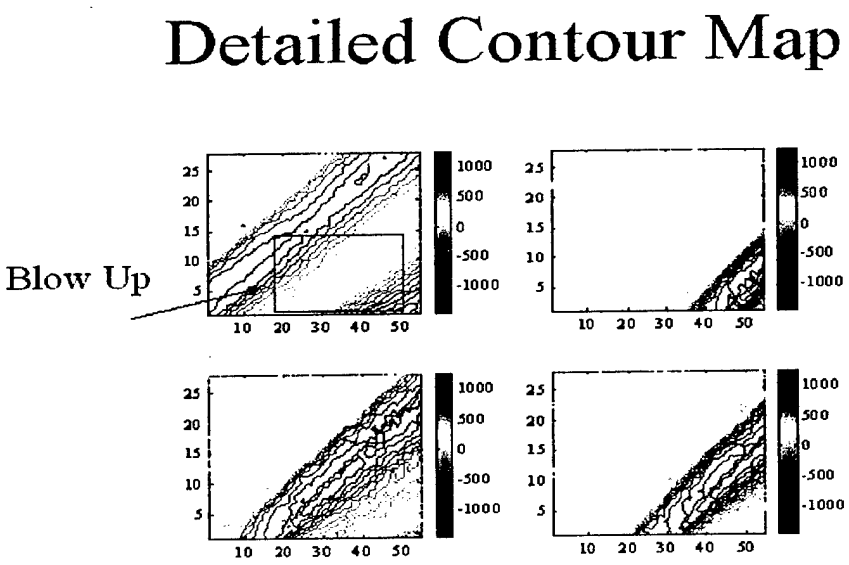

Figure 16. Contour Map of Phase On Top Section Of Projectile

Exploded View

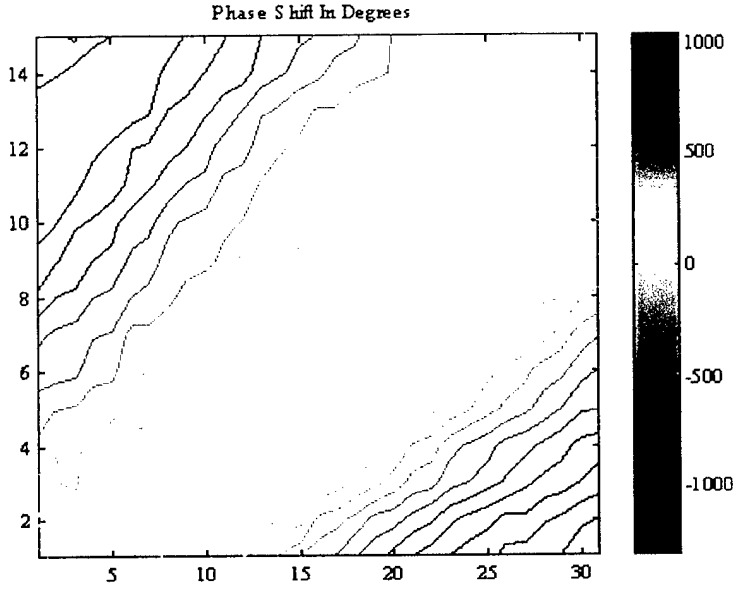

Figure 17. Exploded View Of Phase Contour.

Although this test was of a simple projectile, it highlighted several issues to required for effort and thought. Each issue is discussed below:

Size Of ARF Error Circle – The density station was designed to provide additional insight into the fluid dynamics of experimental projectile of unusual shape. These projectiles are typically sabot launched and then travel down range. The projectile may be 1-6 inches long but more importantly its location down range is typically not known to precision. After repeated design efforts and analysis, it was concluded that the Shack-Hartmann sensor would require an 8" x 8" field of view. While this can be readily performed, it introduced two unexpected results. First, our sensor design was limited to 88 x 88 wavefront sensors in order to accommodate other design issues. While in many applications this would provide exceptional resolution, it does not in the

ARF. Using telescopic optics, the 8 x 8" (203 mm x 203mm) test region is imaged onto the 88 x 88 lenslets. This means that each sensor has a resolution of 2.3 x 2.3 mm, which in turn implies that any flow feature smaller than about 4.6 mm could not be properly resolved. Unfortunately, no resolution was found for this problem since the error in position of the projectile forced the use of such a large aperture. The second unexpected result is the rapid increase in slope of the optical phase front, which in turn causes very large shifts in the spot locations on the detector. The optical wavefront slope increase proportional to the amount of demagnification, which in our case was 23X. Given the large phase changes already present for supersonic projectiles, this proved a tough design constraint.

Complex Shock Structures – For many advanced projectiles of interest at supersonic speeds, there is a very complex shock structure that introduces discontinuities in the Shack –Hartmann data. If these discontinuities are too numerous, it becomes very difficult to reconstruct the optical wavefront.

Moving Flow Field Versus Structure Rate of Change – One of the potential advantages of using this time-resolved wavefront sensor is to monitor unsteady aerodynamics. In a wind tunnel, the image rate of the sensor can be matched to the temporal characteristics of the flow field; these may be on the order of 10's of microseconds. Unfortunately in a free flight facility, 10's of microseconds allow the projectile to fly considerable distance down range. Thus we can only observe unsteady flow over a period equal to the time the projectile is located in the optical window. If this happens to match the time scale of interest for the fluid, then the instrument is useful. Otherwise, we have to gather time images too fast to allow the transient flow field nature to be observed.

Phase Inaccuracy – Using no flow field, we often perform calibration and testing on the instrument. We observed an increase in RMS phase error from 25 degrees in previous instruments to 75 degrees in the current instrument. This required considerable effort to track with nothing producing answers as to the cause. After an extended period of

tracking the problem, we then reconstructed our old optical layout with all the same components (we thought); this still produced the extra phase error.

In the ARF, this extra error was of no consequence because the phase changes where very large. In subsonic applications, however, this produced tremendous problems for use to the point we where no longer able to run cavity testing. Everything was analyzed until finally the origin of the problem was found. In the new lasers we had purchased, there was a facet design change and in addition, we where driving the lasers harder than we had previously. The net effect, in combination with our optical system, was to produce a change in the spot shape profile that was not obvious upon inspection but after later analysis, proved to be the problem. This problem was rectified by switching to the higher power laser diode (but driving with less power).

Once the phase noise issue was identified, we then reevaluated the application of the tomographic sensor in the ARF environment since the large error circle, the large density gradients, and the inability to watch for transient events on time scales of our choosing all led to the decision to switch our effort to apply the system to UF transonic wind tunnel shown in Figure 18.

6. Additional Testing

Additional testing is now underway at the University using the system to study shallow cavities as shown in the picture of Figure 18. The cavity is 1"" in length and 0.1" in depth thus providing an L/D ratio 10. Density measurements obtained from the sensor are shown in Figure 19 for the eight time images, each separated by 50 microseconds. The next step in this project is to look at the flow field from orthogonal directions in a time-synchronized manner.

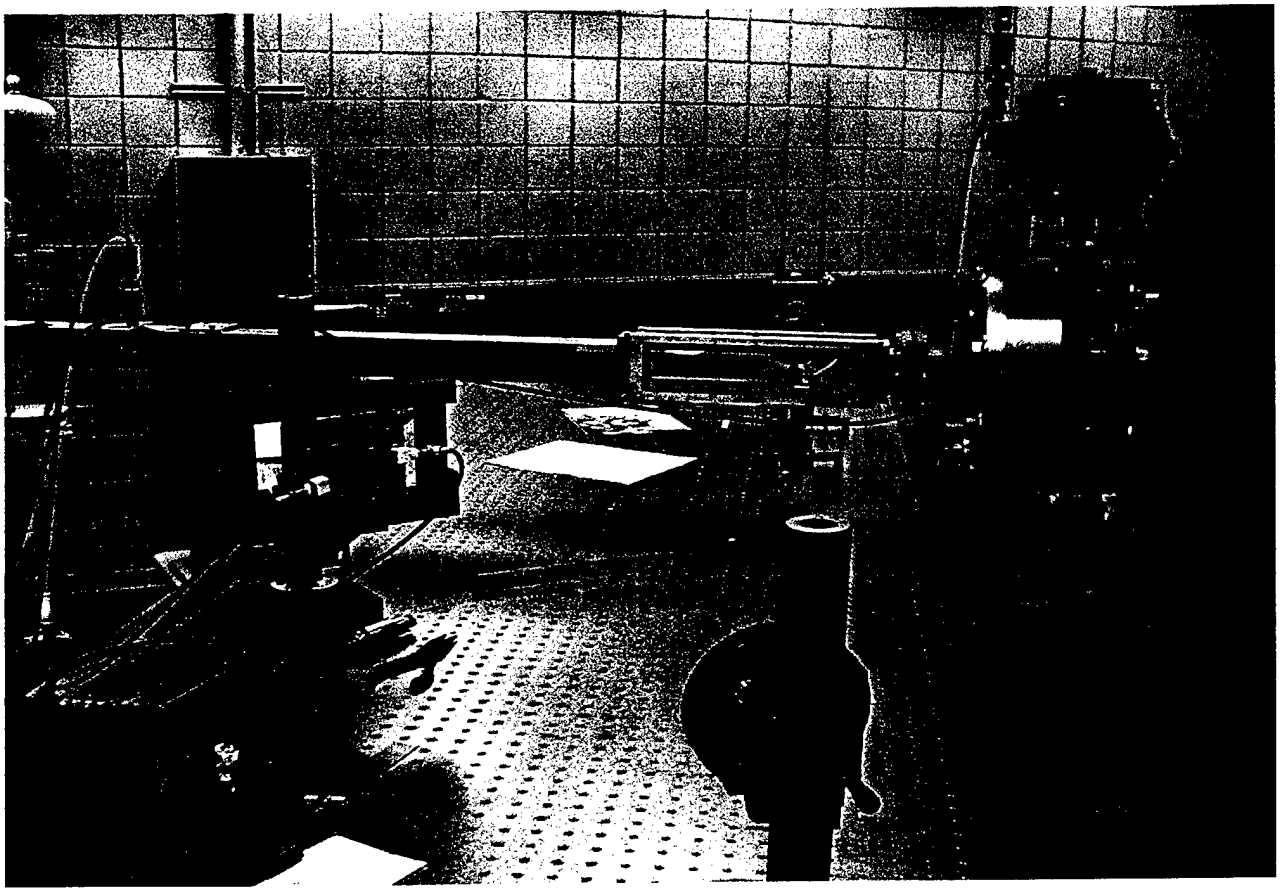

Figure 18. Photograph Of Test Apparatus

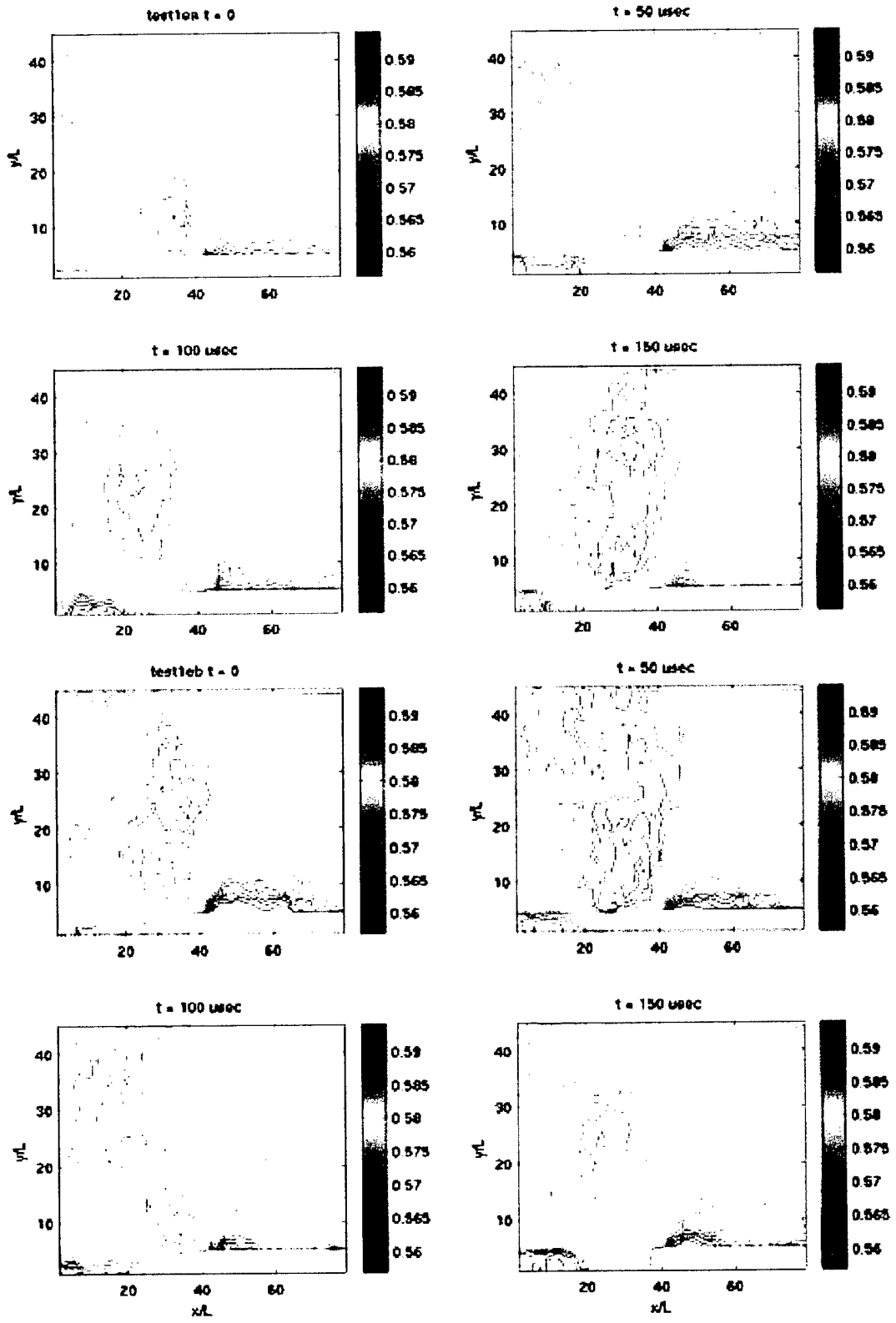

Figure 19. Eight Time Resolved Density Measurements From L/.D=10 Cavity.

7. Conclusions

Equipment has been designed, purchased, and tested for the construction of a density station producing 8 time resolved images with image rates down to 5 microseconds. A synchronized image capture system is in place that allows the capture of 8 time resolved Shack Hartmann images from a total of 10 cameras simultaneously. During the development of this system, considerable insight was gained into suitable applications for the device and those that are not as suitable. We can summarize suitable applications as follows:

1) Flow fields with minimal shock structure;
2) Flow fields with significant temporal changes;
3) Flow fields that do not translate during the desired observation time; i.e., a wind tunnel or combustion type test.
4) Flow fields with density variations much lower than observable by other techniques such as Schlieren or shadowgraph.

In these types of applications, the sensor does a very nice job of accurately measuring the flow field. Our work continues in applying the sensor to a broader class of applications that meet the guidelines above.

8. References

1. J. Land and C. Anderson, "Optical Tomographic Reconstruction Of Fluid Density Using Wavefront Sensor Data", Submitted Applied Optics, May 15, 2000.
2. J. Land, "Shack-Hartmann Wavefront Sensor For Tomographic Reconstruction Of Aerodynamic Flow Density Measurements", University of Florida, Dissertation, 2000.
3. C. Anderson, "Time-Resolved Wavefront Sensor", Patent Disclosure, July2000.
4. W. Merzkirch, "Flow Visualization", 2nd Edition, Academic Press, 1997
5. Abate, Shyy, Anderson, Mikolaitis, Segal, "Time Resolved Flow Visualization Of Shock Waves Undergoing Sudden Expansion", Submitted AIAA, August 1999.
6. G. Abate, "Experimental Investigations of Shock Waves Undergoing Sudden Expansion In a Confined Chamber", University of Florida, Dissertation, 1999.
7. D. Neal, et.al., One dimensional wavefront sensor development for tomographic flow measurements", Proc. SPIE Vol. 2546, pp 378-390, 1995.
8. S. Cha, "Interferometric Tomography of Continous Fields with inccomplete projections", Optics Letters, pp. 299-301, March, 1989.
9. D. Kwo, et. al., "A Hartmann wavefront sensor using a binary optic lenslet array", Proc. SPIE, Vol 1544, pp. 66-74, Nov., 1991.
10. W. Yanta, et. al., Near and Farfield Measurements of Aero-Optical Effects Due to Propagation Through Hypersonic Flows", AIAA 2000-2367.

11. Wavefront Sciences and Adaptive Optics Associaties offers commercially available wavefront sensors based on the Shack-Hartmann approach.
12. L. McMackin, et. al, Hartmann wavefront sensor studies of dynamic orgainized structure in flowfields", AIAA Journal Vol 33, #11, pp. 2158 – 2164, Nov. 1995.

** Note: There have been many other contributions in all aspects of flow field diagnostics, Shack-Hartmann sensors, and tomography. The listed references where kept short in the interest of space.

APPENDIX A SpreadSheet Design

Shack Hartmann Section

Lenslet

f	1.70	mm	Input	
D	100.00	um	Input	
f/#	17.00			
Spot 3 dB Width	13.35	um		
Null Width	26.69	um		
Count	240.00		Input Number Of Lenslets	
Active Dimension	8.81	mm	Detector Size	
Depth of Focus	4.54E-01	mm		Total - Two Sided

Lasers

Wavelength	785.00	nm	Input	
Spacing	5.50	mm	Input	
3 dB Beam Width	5.00	Deg	Input	Min Axis
3 dB Beam Width	20.00	Deg	Input	Max Axis
Output Power	3.00	mW	Input	

Detector

Det. Spacing	8.60	um	ES 1.0/MV	
Det Count	1024.00			
Desired Spot Sep.	[redacted]	Lenslets	Input	
# Det. Lenslet Seperation	11.63	pix		
Desired Spot Sep.	4.65	pix		
Number Pix Per Spot	3.10	Pixels		Null Width
Number Pix Per Spot	1.55	Pixels		3 dB Width

Angles For Multibeam

Time Spots Beam Seperation	0.0235	rads		Angle At Lenslets
Beam Seperation	1.35	Degs		Angle At Lenslets

Transfer Optics

Model

Test Area Size	55.00	mm	Input	Square
Magnification	0.16			
Beam Diameter	77.55	mm		Circular
Beam Diameter	3.05	In		
Lenslet Count	88.06			
Maximum Model Angle Shift	[redacted]	rads	Sort of a Standard Assumption at the model itself	

Angles For Multibeam

Input Beam Sep	0.0038	rads	Demagnification Increases Angle from
Model Shift	0.0018		Should be less than input beam shift
Input Beam Sep	0.22	deg	
Output Beam Sep	0.0235	rads	Simply a Double Check

First Lens

Focal Length	[redacted]	mm	Input	
Operating f/#	10.83			Factors In Square Test Region but rou

Fourier Plane

Spot Seperation	3.30	mm

Seconds Lens

Focal Length	[redacted]	mm	Calculated	
Diameter	12.95	mm		
Operating f/#	10.83			0.221333333

Total Package Length	40.01	Inches	Glass to Glass
	3.33	Feet	

Detector Board

Lasers

Required Distance	1459.88	mm	Nominal
Required Distance	4.79	ft	

Beam Size

Min Axis	127.40	mm	Check to see if we meet the beam requirements